Catalysis Today 148 (2009) 115–118

Contents lists available at ScienceDirect

Catalysis Today

journal homepage: www.elsevier.com/locate/cattod

Oxidation of NO in gas phase by Au–TiO_2 photocatalysts prepared by the sol–gel method

J. Hernández-Fernández [a,b,*], A. Aguilar-Elguezabal [a], S. Castillo [b], B. Ceron-Ceron [b], R.D. Arizabalo [b], M. Moran-Pineda [b]

[a] Centro de Investigación en Materiales Avanzados, Av. Miguel de Cervantes #120, Complejo Industrial, C.P. 31109, Chihuahua, Chih., Mexico
[b] Instituto Mexicano del Petróleo, Dirección de Investigación y Posgrado, Eje Central Lázaro Cárdenas, No. 152, C.P. 07730, D.F., Mexico

ARTICLE INFO

Article history:
Available online 3 June 2009

Keywords:
Titanium dioxide
Gold
Sol–gel
Photocatalysis

ABSTRACT

This work describes an innovative nanosemiconductor system, based on Au–TiO_2 for UV photo-assisted oxidation of nitrogen monoxide (NO). The synthesis of these materials was carried out by the sol–gel method. Titanium(IV) isopropoxide and $HAuCl_4$ were the precursors of the photocatalyst, which was prepared in acid conditions. The catalysts were characterized by the following techniques: BET, XRD, UV–vis and dark-field TEM. The evaluation of the photocatalytic activity was performed *in situ* using an FTIR spectrometer with high sensitivity and a UV spectrometer (365 nm) after 60 min at atmospheric pressure and room temperature. The NO + O_2 mixture concentration was 150 ppm. The photocatalytic conversion of nitrogen monoxide (NO) was studied by FTIR, which reached 85% in 60 min. The semiconductor type materials exhibited an enhanced photoactivity when compared with our reference TiO_2.

© 2009 Elsevier B.V. All rights reserved.

1. Introduction

Nanostructured materials offer promising opportunities for the synthesis of new materials with improved properties. Due to the control of the steady particle size and the crystalline phase that can be obtained, the sol–gel method is considered as one of the most versatile procedures in comparison with other chemical or physicochemical methods [1–3]. TiO_2 is an n-type semiconductor, with a band gap of 3.2 eV, which presents three crystalline phases: brookite, anatase and rutile [4–6]. The anatase crystalline phase shows, in general, a photoactivity which is better than that of the rutile phase. In order to increase the photocatalytic activity, the TiO_2 surface has been modified by doping it with metallic ions such as gold. Gold has recently become of great interest due to its good activity in the degradation of contaminants. This improved photocatalytic activity depends on the support, the size and distribution of the gold nanoparticles and the properties of the contact surface [7–12]. Nitrogen oxides (NO_x) are atmospheric pollutants due to their role concerning not only the generation of photochemical smog and acid rain but also the promotion of the ozone formation [13]. The photocatalytic oxidation of NO over TiO_2 and Au/TiO_2 under different reaction conditions has been reported in the literature [14–18]. However, one of the most important goals is to obtain catalysts with photocatalytic properties. Among the applied techniques one can find: impregnation by flame spray pyrolysis, wet-chemistry, solvated metal atom impregnation, deposition–precipitation and sol–gel [19–23]. In this work, Au–TiO_2 nanostructured photocatalysts were prepared by the sol–gel method. The synthesis, characterization of the obtained structures, morphology, band gap energy and gold particle sizes were analyzed. The photoactivity was evaluated *in situ* by using mixtures of NO and O_2, using a ultraviolet light source of 365 nm.

2. Experimental

2.1. Preparation of the Au–TiO_2 nanoparticles

The catalysts were prepared by the controlled sol–gel method as follows: titanium tetraisopropoxide (Aldrich), $HAuCl_4$ (0.5, 1.0 and 3.0 wt%), was dissolved in 2-propanol (J.T. Baker 9000-03) and distilled water. The solution was refluxed at 70 °C under constant stirring until the gel was formed. The formation of the gels was obtained by controlled hydrolysis-condensation reactions at 70 °C for 24 h at pH 3. Afterwards, the solids were dried in an oven for 12 h at 80 °C. Finally, the excess solvent and water were removed at 300 °C for 4.5 h, using a 2 °C/min heating rate. After activation,

* Corresponding autor at: Centro de Investigación en Materiales Avanzados, Av. Miguel de Cervantes #120, Complejo Industrial, C.P. 31109, Chihuahua, Chih., Mexico.
E-mail addresses: javier.fernandez@cimav.edu.mx (J. Hernández-Fernández), fmarina@imp.mx (M. Moran-Pineda).

0920-5861/$ – see front matter © 2009 Elsevier B.V. All rights reserved.
doi:10.1016/j.cattod.2009.04.019

Table 1
Specific surface areas, band gap energy and photocatalytic activity of the studied materials.

Catalyst	BET (m^2/g)	E_g (eV)	NO removal after 60 min (%)
TiO_2	161.8	3.13	70
Au/TiO_2 0.5%	129.5	2.93	85
Au/TiO_2 1.0%	114	2.83	81
Au/TiO_2 3.0%	100.4	2.86	78

the catalysts were reduced in hydrogen flow (100 ml/min) at 300 °C for 4 h.

2.2. Characterization of the materials

The specific surface area of the obtained materials was determined by N_2 adsorption by means of a Quantachrome sorptmeter. The specific surface area (BET) and the pore size distribution were calculated from the N_2 absorption–desorption isotherms. The crystalline phase was determined by X-ray diffraction (XRD) with a Bruker D-8 diffractometer using Cu Kα radiation with a 2θ step of 0.03. The transmission electron microscopy (TEM) studies were performed with a JEM-2200FS equipment with an acceleration voltage of 200 kV. The local chemical analysis and the chemical mapping were performed by means of an energy-dispersion X-ray spectrometer (EDXS) NORAN spectrometer, which is coupled to a microscope allowing the STEM-EDX combination. High-angle annular dark-field scanning transmission electron microscopy (HAADF-STEM) was also performed. The UV–vis spectra (200–900 nm) of the materials were obtained with an UV–vis Varian Cary 100 spectrometer (diffuse reflectance). The band gap of the solids was calculated by linearization of the slope with respect to the *x*-axis for *y*-axis equal to 0.

2.3. Evaluation of the photocatalytic activity

An *in situ* type photoreactor was built to study photocatalytic reactions using a variety of gases and gas mixtures. The photoreactor, with a length of 20 cm, has potassium bromide (KBr) windows on its opposite sides. The aforementioned characteristics allow to place it inside the equipment chamber to perform the reaction and obtain real-time measurements. The system also has a vacuum system to remove the gases in the cell, and an air purge system that creates a clean atmosphere inside the reactor chamber. The evaluation of the photocatalytic activity was performed by means of a Bruker IFS66 v/S spectrometer equipped with an MCT (mercury–cadmium–tellurium) high sensitivity detector with a resolution of 0.5 cm^{-1} and an optical step of 25 cm^{-1}. A $NO–O_2$ mixture was admitted with a concentration of NO of 150 ppm, which was irradiated with an UV light of 365 nm. The UV lamp was horizontally placed at the upper part of the reactor, 10 cm from both ends. The evaluation was carried out by using 100 mg of catalyst for 60 min at atmospheric pressure and room temperature. The spectra were developed within the range going from 4000 to 400 cm^{-1}, and monitored every 4 min.

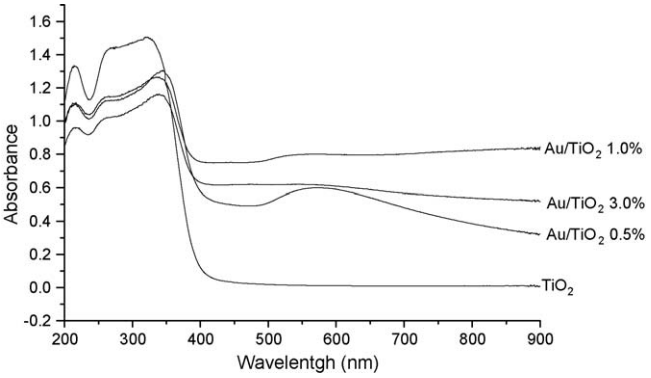

Fig. 2. UV–vis diffuse absorbance spectra of the semiconductors.

3. Results and discussion

The specific surface areas obtained on the synthesized materials are reported in Table 1. For the bare catalyst (TiO_2), it was equal to 161.8 m^2/g, whereas those of the catalysts doped with gold (0.5, 1.0 and 3.0 wt%) were 129.5, 114.0 and 100.4 m^2/g, respectively. These results show that the specific surface area of the support was modified with gold.

The X-ray diffraction patterns of the catalysts calcined at 300 °C are shown in Fig. 1; the spectra show the five characteristic diffraction peaks of the titania anatase phase. Additionally, it can also be observed at around $2\theta = 31°$, the peak assigned to the brookite phase. The diffraction patterns show the anatase crystalline phase in a higher proportion with respect to that of brookite. The presence of gold can be identified in the diffractograms at around the 2θ peaks = 44°, 64° and 78°, respectively.

The diffuse absorption spectra of the materials are shown in Fig. 2. The diffuse reflectance measurements in the UV–vis region enabled us to determine the band gap energy of the semiconductors by extrapolation to the energy axis of the linear interval in a plot $(\alpha h\nu)^2$ *vs* $h\nu$ [24]. The band gap energy values obtained in this way for the bare and doped TiO_2 materials are summarized in Table 1. The TiO_2 band gap appears in the 380–459 nm region; the band widening in the 520–680 nm region can be noticed for the catalysts doped with gold. The resonance band concerning the gold Plasmon is associated with gold particles that are larger than 5 nm [25].

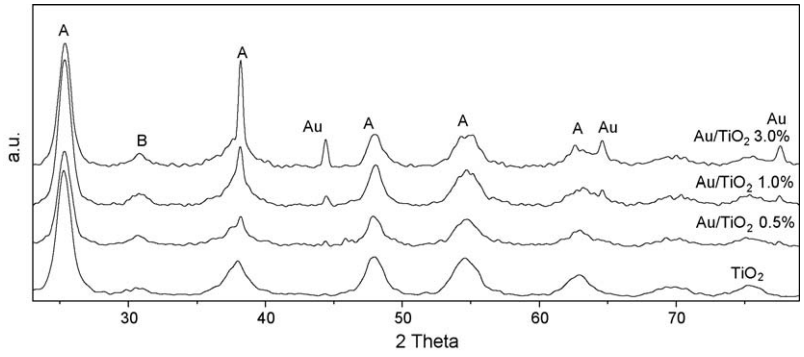

Fig. 1. XRD diffraction patterns of the materials. Reflections due to anatase, brookite and gold are labeled as (A), (B) and (C), respectively.

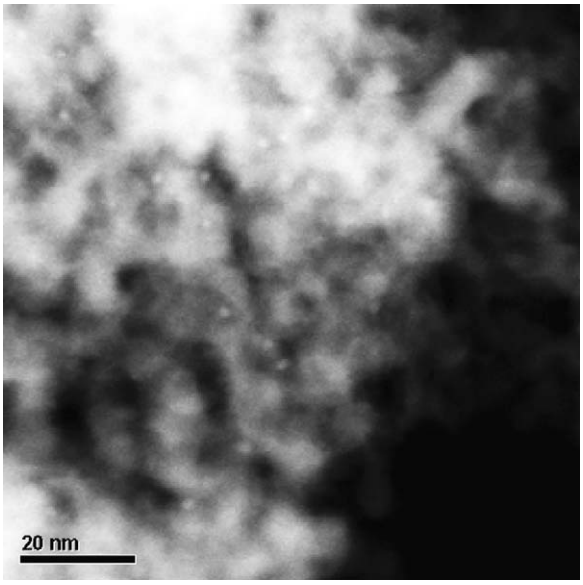

Fig. 3. Dark-field TEM micrograph of the Au–TiO_2 (1.0 wt%).

Dark-field TEM imaging was used to study the particle size distribution and morphology of the materials. In Fig. 3, the bright spots and areas in the dark-field image indicate the presence of gold particles and anatase nanocrystallites in the Au–TiO_2 (1.0 wt%) catalyst. The EDX analyses show the presence of gold, titanium and oxygen as part of the composition of the material. The presence of copper in the analysis corresponds to the grid used in the microscope (Fig. 4).

The NO in an oxygen-rich mixture shows a photocatalytic conversion profile after 60 min, Fig. 5. It can be seen that the Au–TiO_2 (0.5 wt%) catalyst shows a conversion of 85%; the Au–TiO_2 (1.0 wt%), 81%; the Au–TiO_2 (3.0 wt%), 78%; and the bare TiO_2, 70%.

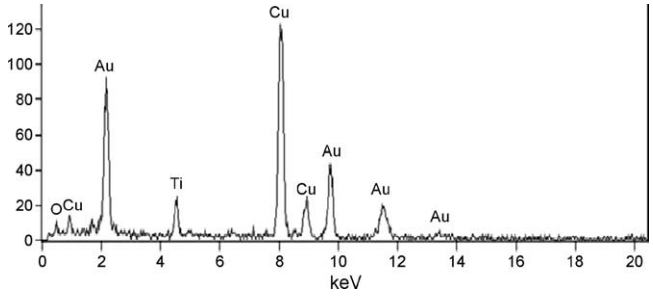

Fig. 4. EDX of Au–TiO_2 (1.0 wt%).

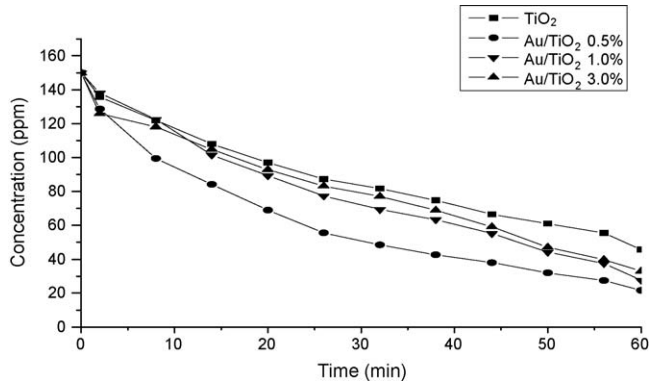

Fig. 5. Profile of the percentage of nitric oxide decomposed for 60 min under UV irradiation.

The high photoactivity of the synthesized catalysts can be related to the gold particles in the nanometric range. According to the photocatalytic activity, the highest reactivity seems to be mainly related to the pure anatase phase of the sample and it was found that gold deposited on the titania supports notably increased the NO conversion, N_2O was the major reaction product under the experimental oxidation conditions in this work, these two properties have been previously pointed out as important factors for photocatalytic reactions by other authors [26,27]. The role of the gold particles can be attributed to a diminution of the e^-/h^+ pair recombination rate, which improves the photocatalytic activity.

According to Bowering et al. [14], the reaction route could follow the following steps:

$$TiO_2 + h\nu \rightarrow e^- + h^+ \quad (1)$$

$$NO + e^- \rightarrow N + O \quad (2)$$

$$NO + N \rightarrow N_2O \quad (3)$$

$$NO + O \rightarrow NO_2 \quad (4)$$

$$2O \rightarrow O_2 \quad (5)$$

$$2N \rightarrow N_2 \quad (6)$$

$$2NO \rightarrow N_2 + O_2 \quad (7)$$

$$N_2O \rightarrow N_2 + O \quad (8)$$

4. Conclusions

In the present work, the preparation of TiO_2 and Au doped titania by the sol–gel method was performed. The obtained catalysts, annealed at 300 °C, show specific surface areas between 100.4 and 161.8 m^2/g, The E_g values of the various samples, doped and un-doped, are similar to those reported for anatase. Such results indicate that the doping of titania with Au exerts little effect on the band gap in comparison with our reference preparation. It was found that gold shifts the band gap energy to lower energy values. The Plasmon intensity band was observed in the UV–vis spectra for the catalysts one with an Au content of 0.5 and 1%. Nanosized gold particles lesser than 10 nm were obtained by the sol–gel method. By testing the catalysts in the NO reaction, it was shown that the most efficient photocatalysts for the oxidation were obtained when the gold nanoparticles were deposited on the TiO_2 supports. The catalyst that showed the best performance was the one with an Au content of 0.5%, and the lowest performance was shown by the bare TiO_2.

Acknowledgments

The authors want to thank the support provided by both the Instituto Mexicano del Petróleo (IMP) and Consejo Nacional de Ciencia y Tecnología (CONACYT). The technical assistance by Rufino Velázquez Lara (IMP) has been of great importance to this work.

References

[1] R.S. Sonawane, M.K. Dongare, Journal of Molecular Catalysis A: Chemical 243 (2006) 68.
[2] Y. Chen, D.D. Dionysiou, Applied Catalysis B: Environmental 62 (2006) 255.
[3] A.K. Subramani, K. Byrappa, G.N. Kumaraswamy, H.B. Ravikumar, C. Ranganathaianh, K.M. Lokanatha Rai, S. Ananda, M. Yoshimura, Materials Letters 61 (2007) 4828.

[4] Z.Y. Yuan, B.L. Su, Colloids and Surfaces A: Physicochemical and Engineering Aspects 241 (2004) 173.
[5] S. Watson, D. Beydoun, D. Scott, R. Amal, Journal of Nanoparticles Research 6 (2004) 193.
[6] A.G. Agrios, P. Pichat, Journal of Applied Electrochemistry 35 (2005) 655.
[7] A. Mirescu, H. Berndt, A. Martin, Ulf Prube, Applied Catalysis A: General 317 (2007) 204.
[8] F. Moreau, G.C. Bond, Applied Catalysis A: General 302 (2006) 110.
[9] M.A. Centeno, M. Paulis, M. Montes, J.A. Odriozola, Applied Catalysis B: Environmental 61 (2005) 177.
[10] B. Schumacher, V. Plzak, J. Cai, R.J. Behm, Catalysis Letters 101 (2005) 215.
[11] G.J. Hutchings, Catalysis Today 122 (2007) 196.
[12] S. Zhang, Q. Yu, Z. Chen, Y. Li, Y. You, Materials Letters 61 (2007) 4839.
[13] F.B. Li, X.Z. Li, C.H. Ao, M.F. Hou, S.C. Lee, Applied Catalysis B: Environmental 54 (2004) 275.
[14] N. Bowering, G.S. Walter, P.G. Harrison, Applied Catalysis B: Environmental 62 (2006) 208.
[15] J. Zhang, T. Asuyama, M. Minagawa, K. Kinugawa, H. Yamashita, M. Matsuoka, M. Anpo, Journal of Catalysis 198 (2002) 1.
[16] J.S. Dalton, P.A. Janes, N.G. Jones, J.A. Nicholson, K.R. Hallam, G.C. Allen, Environmental Pollution 120 (2002) 415.
[17] C.H. Ao, S.C. Lee, C.L. Mark, L.Y. Chan, Applied Catalysis B: Environmental 42 (2003) 119.
[18] M.A. Debeila, N.J. Coville, M.S. Scurrell, G.R. Hearne, M.J. Witcomb, Journal of Physical Chemistry B 108 (2004) 18524.
[19] G.L. Chiarello, E. Selli, L. Forni, Applied Catalysis B: Environmental 84 (2008) 332.
[20] B. Tian, C. Li, F. Gu, H. Jiang, Catalysis Communication 10 (2009) 925.
[21] S.H. Wu, X.C. Zheng, S.R. Wang, D.Z. Han, W.P. Huang, S.M. Zhang, Catalysis Letters 97 (2004) 17.
[22] R. Zanella, L. Delannoy, C. Louis, Applied Catalysis A: General 292 (2005) 62.
[23] V. Meille, Applied Catalysis A: General 315 (2006) 1.
[24] S.D. Mo, W.Y. Ching, Physical Review B 51 (1995) 13023.
[25] P.V. Kamat, Journal of Physical Chemistry B 106 (2002) 7729.
[26] L. Cao, Z. Gao, S.L. Suib, T.N. Obee, S.O. Hay, J.D. Freihaut, Journal of Catalysis 196 (2000) 253.
[27] A.J. Maira, J.M. Coronado, V. Augugliaro, K.L. Yeung, J.C. Conesa, J. Soria, Journal of Catalysis 202 (2001) 413.